Electronic Supplementary Material (ESI) for Inorganic Chemistry Frontiers.

Supplementary Information

Hydrogen Production from Complete Dehydrogenation of Hydrazine Borane on Carbon-doped TiO_2-supported NiCr Catalysts

Xiaolei Zhang, Qilu Yao,* Yuzhao Wang, Mengying Liu, Zhang-Hui Lu*

Institute of Advanced Materials (IAM), Key Laboratory of Energy Catalysis and Conversion of Nanchang, College of Chemistry and Chemical Engineering, Jiangxi Normal University, Nanchang 330022, China

*E-mail: yaoqilu@jxnu.edu.cn (Q. Yao); luzh@jxnu.edu.cn (Z.-H. Lu)

Table of Contents

Experimental section

Materials and reagents: All the chemicals were analytical purity and used without further purifications. Pluronic F127 ($PEO_{106}PPO_{70}PEO_{106}$, Mw = 12600 g/mol, Acros Corp.), acetic acid (CH_3COOH, Tianjin ZhiYuan Reagent Co., Ltd., AR), hydrochloric acid (HCl, Nanchang Chemical Works, 36~37wt%), tetrahydrofuran (THF, Tianjin ZhiYuan Reagent Co., Ltd., AR), tetrabutyl titanate (TBOT, aladdin Biochemical Technology Co., Ltd., 98.0%), ethanol (C_2H_5OH, Tianjin ZhiYuan Reagent Co., Ltd., AR), glycerol ($C_3H_8O_3$, XILONG Scientific Co., Ltd., AR), nickel chloride hexahydrate ($NiCl_2{\cdot}6H_2O$, Sinopharm Chemical Reagent Co., Ltd, ≥98.0%), chromium(III) nitrate nonahydrate ($Cr(NO_3)_3{\cdot}9H_2O$, Aladdin, 98.0%), sodium borohydride ($NaBH_4$, J&K Chemical, 98.0%), sodium hydroxide (NaOH, Tianjin Zhiyuan Chemical Reagent Co., Ltd,≥96.0%), hydrous hydrazine ($N_2H_4{\cdot}H_2O$, Aladdin, 98%,), and hydrazine hemisulfate salt ($N_2H_4{\cdot}1/2H_2SO_4$, Aldrich, 99.5%) were used without further purification. Ultrapure water used in the experiment was purified using a Millipore system.

Syntheses of hydrazine borane: Hydrazine borane ($N_2H_4BH_3$) was synthesized according to our previous work [S1,S2]. Typically, 21.42 g of hydrazine hemisulfate salt ($N_2H_4{\cdot}1/2H_2SO_4$) and 10.0 g of sodium borohydride ($NaBH_4$) were added into 160 mL of anhydrous 1,4-dioxane with stirring at 303 K under an atmosphere of dry argon for 48 h. The resulting slurry was then centrifuged to get the clear solution, and then the filtrate was dried in a rotary evaporator at 333 K overnight. The obtained raw $N_2H_4BH_3$ was further washed with n-pentene, then the white solid-state $N_2H_4BH_3$ was finally obtained after drying under vacuum at 313 K.

Catalytic activity measurement: The reaction device for measuring $N_2H_4BH_3$ gas production is the same as described in our previous work [S3]. Usually, a catalyst suspension solution (5 mL) in the two-neck round-bottomed flask (50 mL). Immerse the flask in a constant temperature water bath. One of the two necks is used to connect the gas burette to the measure the volume of released gas. The other neck is used to

inject $N_2H_4BH_3$ (1.0 mmol) into the catalyst suspension under stirring, and the decomposition reaction begins. The volume of gas released is measured by recording the displacement of water in the gas burette. The content of Ni was fixed to be nNi/$n$$N_2H_4BH_3$ of 0.2 for all the catalysts.

Characterization： The detailed morphology and microstructures of the synthesized samples were investigated by scanning electron microscope (SEM, SU8020) and transmission electron microscopy (TEM, JEM-2100) coupled with an energy dispersive X-ray (EDX) detector for elemental analysis. Powder X-ray diffraction (XRD) patterns were carried out with X-ray diffractometer of Rigaku Rint-2200, using graphite monochromatized Cu Kα radiation (λ = 1.54 Å) at a scanning rate of 4°/min. The phase composition and crystallinity of samples were investigated by Raman (LabRAM HR Evolution). Thermogravimetry analysis was conducted on a Mettler Toledo TGA/SDTA851 analyzer from 30 to 800 °C in the air (20 mL/min) with a ramp rate of 5 °C/min. Fourier transform infrared (FTIR) spectra were carried on a Thermo Nicolet 6700 instrument. Electron paramagnetic resonance (EPR) was carried out by using Bruker A300 at 77 K. The UV-Vis absorption spectra were recorded by UV-Vis spectrophotometer (UV-Vis, Hitachi, U-3310) from the scale range of 400-700 nm. X-ray photoelectron spectroscopic (XPS) spectra were collected on a Thermo Scientific ESCALABMKLL apparatus using an Al Kα source. The Ar sputtering experiment was taken under a sputtering acceleration voltage of 1 kV and a background vacuum 3.2×10^{-6} Pa. The Brunauer-Emmett-Teller (BET) equation method was used to analyze the specific surface areas, on the basis of nitrogen adsorption-desorption isotherms which was recorded on a BELSORP-mini II at 77 K. The sample was degassed at 423 K for 12 h before analysis. Determine the gas composition by using a gas chromatograph (GC-9790Plus).

Calculation method: The H_2 selectivity for $N_2H_4BH_3$ (α) dehydrogenation is calculated by the following reaction formulas (Eqs. (S1-S2):

$$N_2H_4BH_3 + 3H_2O \rightarrow B(OH)_3 + (3 + 2\alpha)\, H_2 + (2\alpha+1)/3\, N_2 + 4(1-\alpha)/3NH_3 \qquad (S1)$$

$$\alpha = \frac{3\lambda - 10}{8}\left[\lambda = \frac{n(H_2 + N_2)}{n(N_2H_4BH_3)}\left(\frac{10}{3} \leq \lambda \leq 6\right)\right] \qquad (S2)$$

The turn over frequency (*TOF*) reported in this work is an apparent *TOF* value based on the number of metal Ni atoms in catalysts, which is calculated from the equation as follow:

$$TOF = \frac{n(H_2)}{n(metal) \times t} \qquad (S3)$$

Where nH_2 is the mole number of generated H_2, *n*metal is the total mole number of Ni in catalyst and *t* is the completed reaction time in hour.

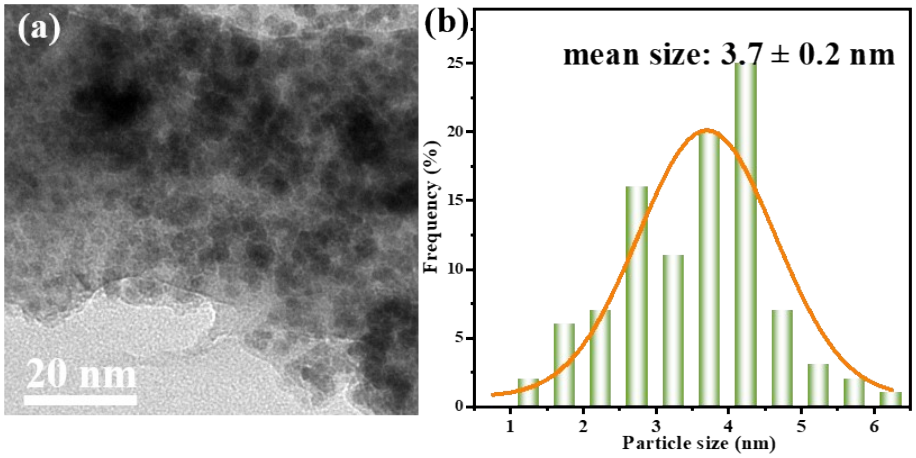

Fig. S1. TEM image and the corresponding particle size distribution of Ni/CTO-NF.

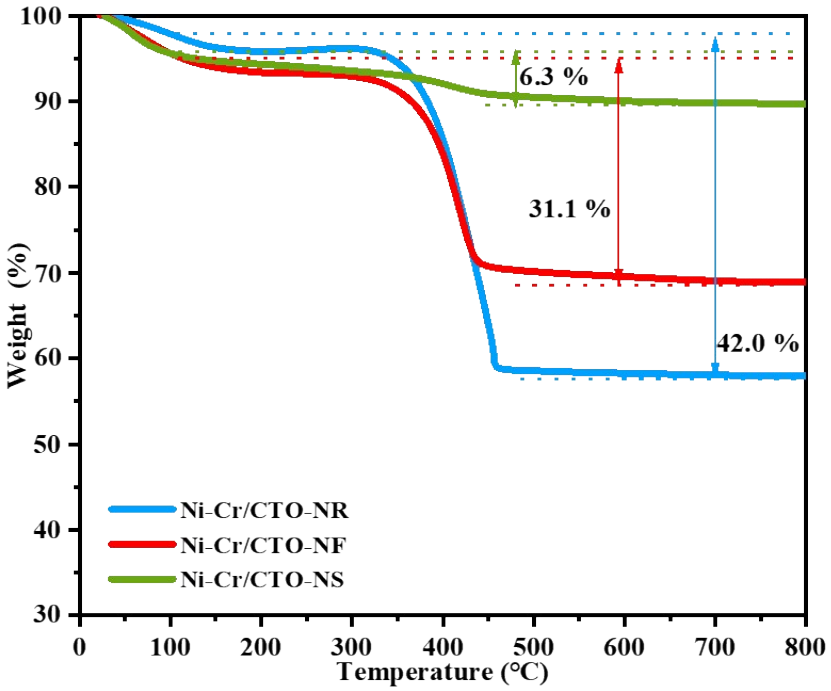

Fig. S2. TG curves of the Ni-Cr/CTO-NS, Ni-Cr/CTO-NF, and Ni-Cr/CTO-NR.

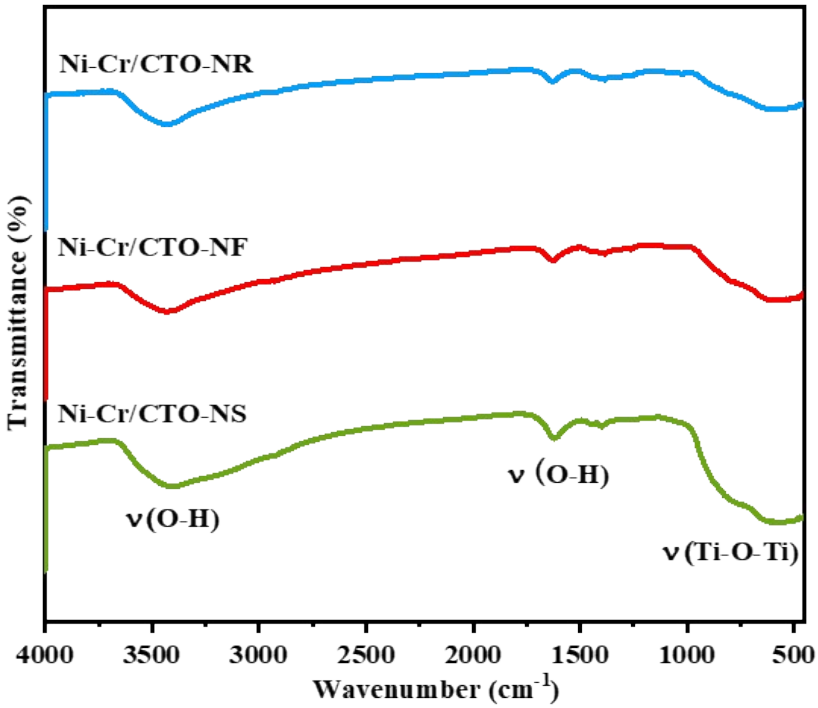

Fig. S3. FTIR spectra of the Ni-Cr/CTO-NS, Ni-Cr/CTO-NF, and Ni-Cr/CTO-NR.

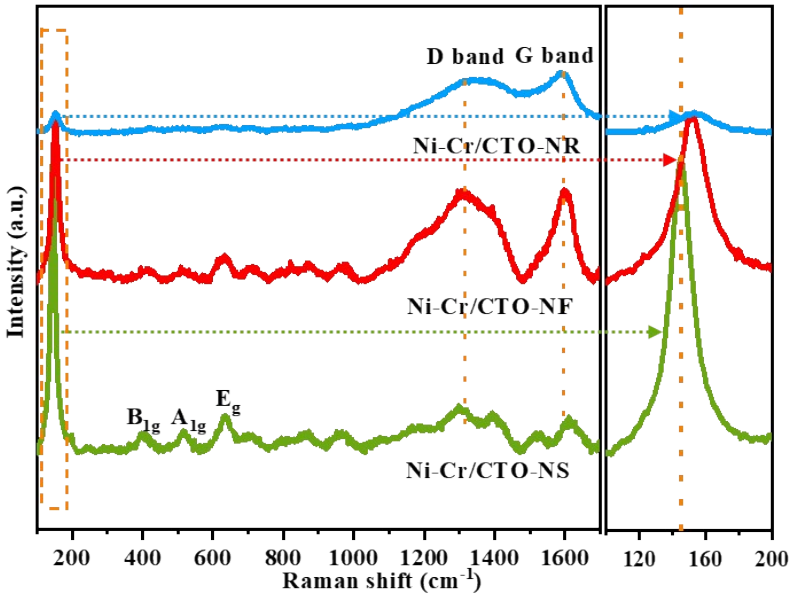

Fig. S4. Raman spectra of Ni-Cr/CTO-NS, Ni-Cr/CTO-NF, and Ni-Cr/CTO-NR.

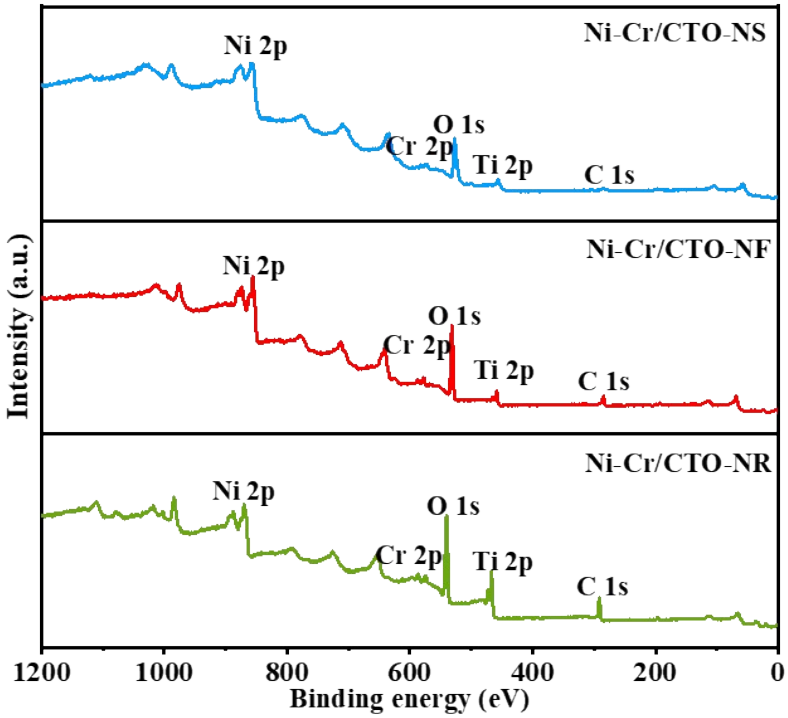

Fig. S5. The survey XPS spectra of the Ni-Cr/CTO-NS, Ni-Cr/CTO-NF, and Ni-Cr/CTO-NR.

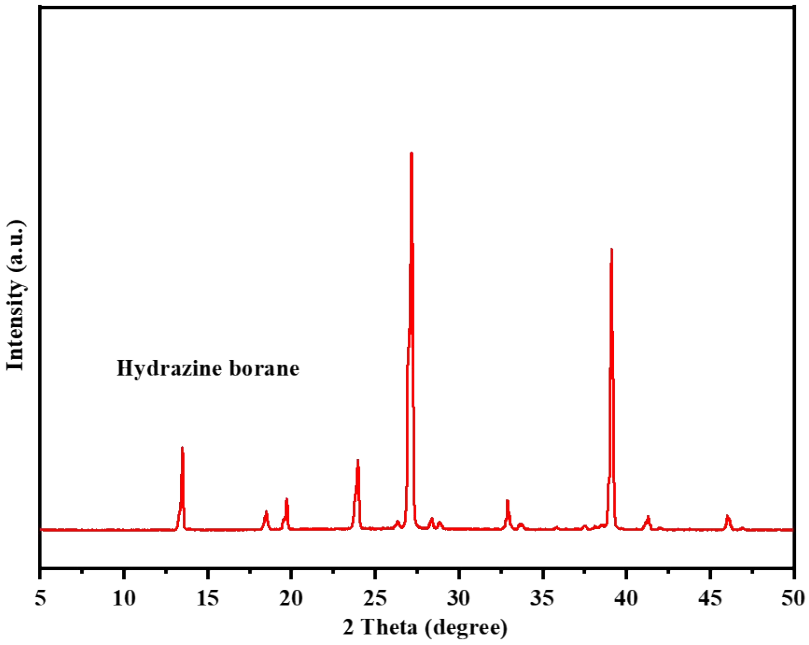

Fig. S6. The XRD pattern of synthesized $N_2H_4BH_3$.

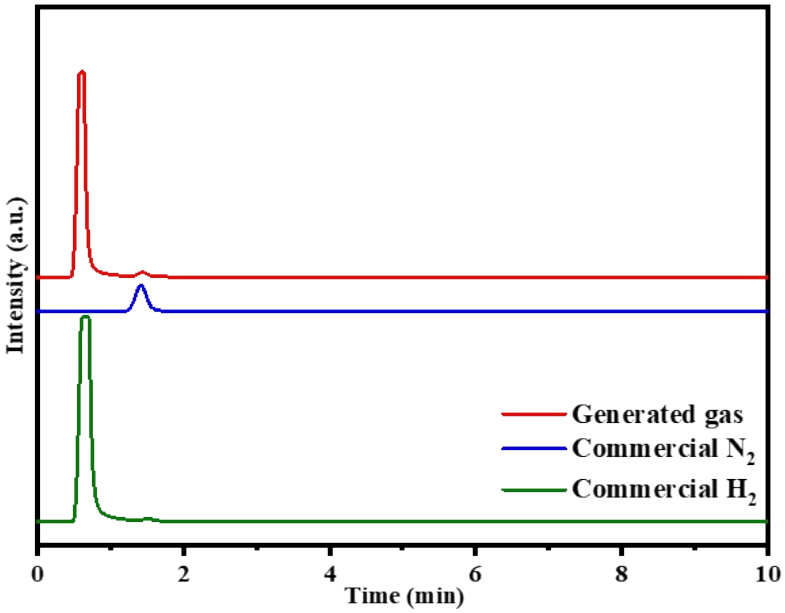

Fig. S7. GC analysis of the released gases from the decomposition of $N_2H_4BH_3$.

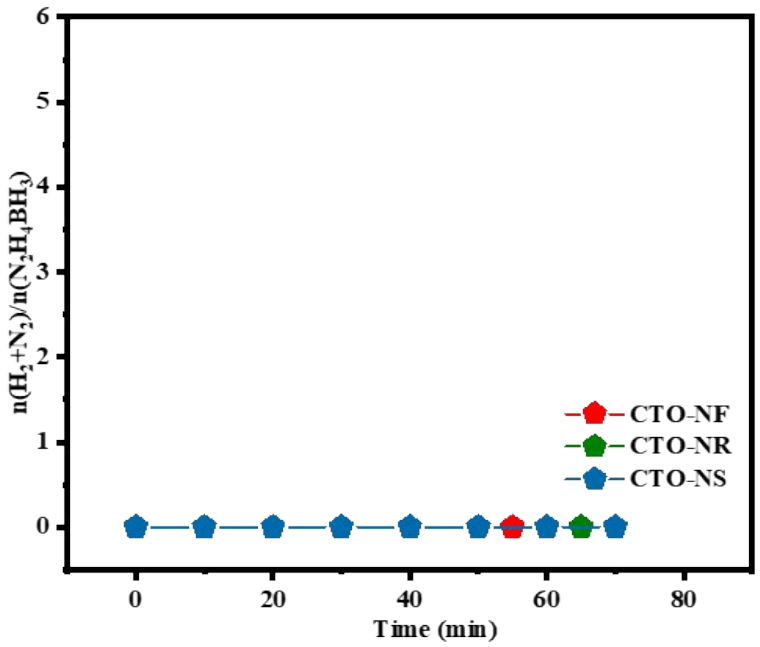

Fig. S8. Time course plots for hydrogen evolution from aqueous $N_2H_4BH_3$ solution (0.2 M, 5 mL) over CTO with different morphologies in the presence of NaOH (3.0 M) at 323 K.

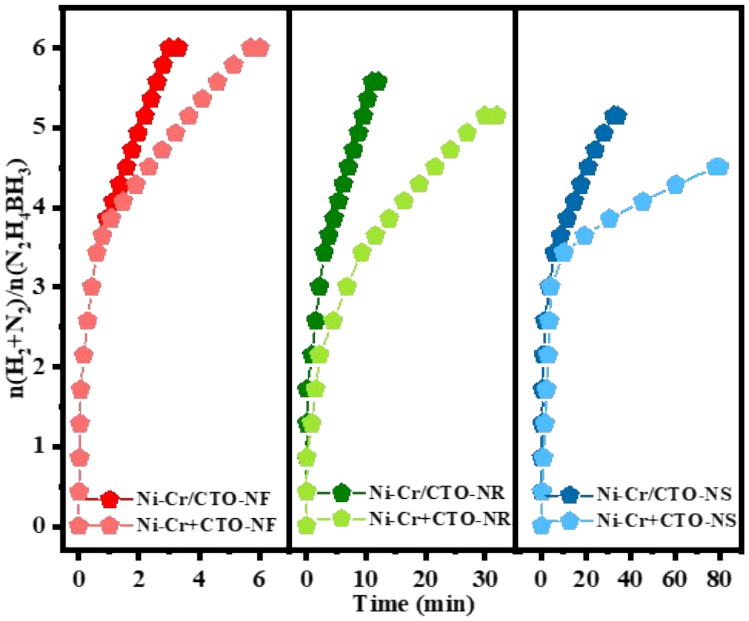

Fig. S9. Time course plots for hydrogen evolution from aqueous $N_2H_4BH_3$ solution (0.2 M, 5 mL) over Ni-Cr/CTO-NF, Ni-Cr + CTO-NF, Ni-Cr/CTO-NR, Ni-Cr + CTO-NR, Ni-Cr/CTO-NS, and Ni-Cr + CTO-NS in the presence of NaOH at 323 K ($n_{Ni}/n_{N2H4BH3}$ = 0.2).

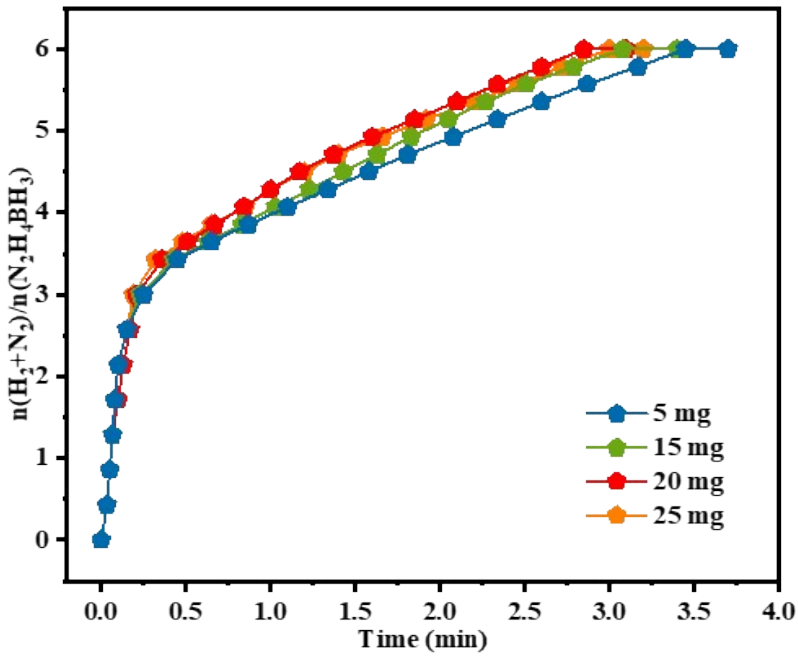

Fig. S10. Time course plots for hydrogen release from aqueous $N_2H_4BH_3$ solution (0.2 M, 5 mL) over Ni-Cr/CTO-NF with different amounts of CTO in the presence of NaOH (3.0 M) at 323 K ($n_{Ni}/n_{N2H4BH3}$ = 0.2).

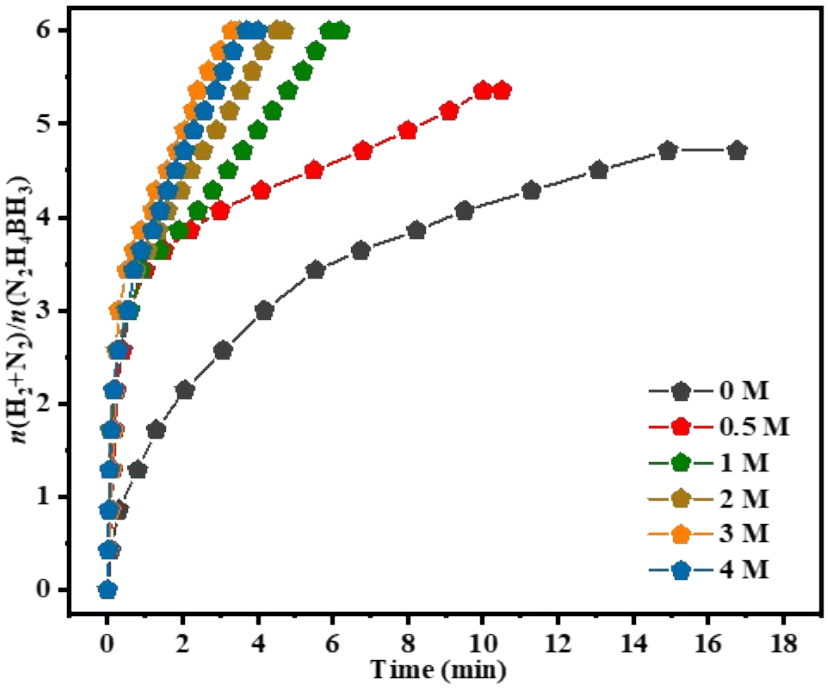

Fig. S11. Time course plots for hydrogen release from aqueous $N_2H_4BH_3$ solution (0.2 M, 5 mL) over Ni-Cr/CTO-NF with different concentrations of NaOH at 323 K ($n_{Ni}/n_{N2H4BH3}$ = 0.2).

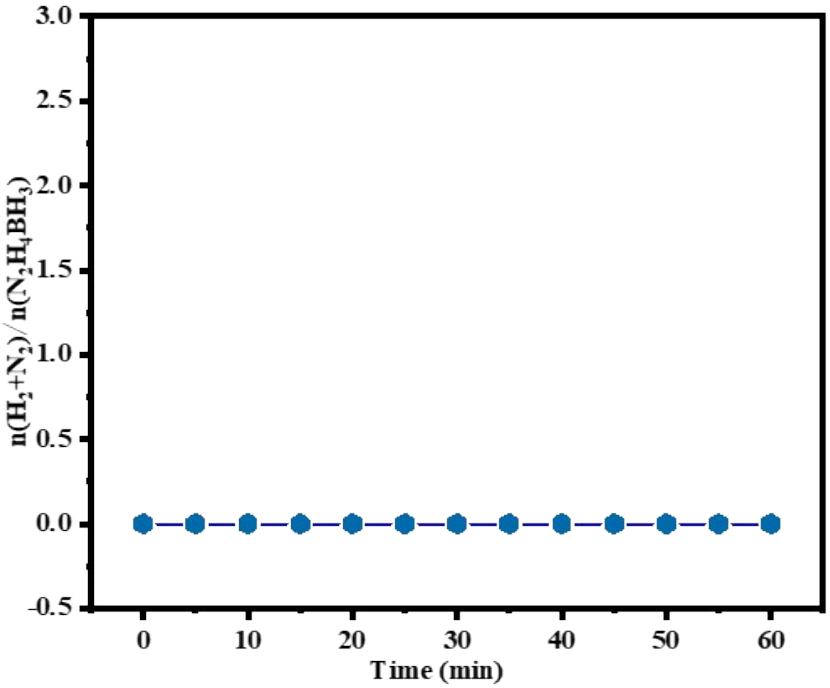

Fig. S12. Time course plots for hydrogen release from aqueous $N_2H_4BH_3$ solution (0.2 M, 5 mL) in the presence of NaOH (3.0 M) without catalyst at 323 K ($n_{Ni}/n_{N2H4BH3}$ = 0.2).

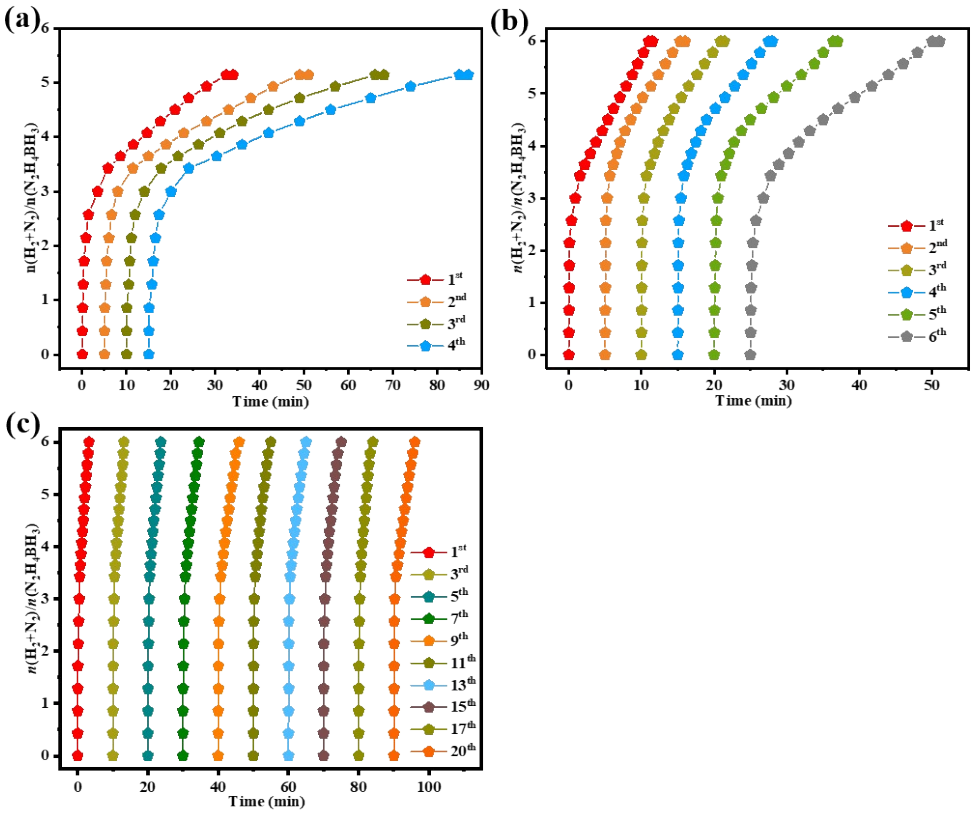

Fig. S13. Stability test for dehydrogenation of aqueous $N_2H_4BH_3$ solution (0.2 M, 5 mL) over (a) Ni-Cr/CTO-NS, (b) Ni-Cr/CTO-NR, and (c) Ni-Cr/CTO-NF with NaOH at 323 K ($n_{Ni}/n_{N2H4BH3}$ = 0.2).

Table S1. The specific surface area, pore volume, and average pore diameter of different samples.

Catalysts	BET surface area (m^2 g^{-1})	Pore Volume (cm^3 g^{-1})	Average pore Diameter (nm)
Ni-Cr/CTO-NS	20.5	0.102	8.7
Ni-Cr/CTO-NR	37.5	0.176	16.5
Ni-Cr/CTO-NF	45.7	0.192	18.3

Table S2. Comparison of the catalytic activities for hydrogen evolution from aqueous $N_2H_4BH_3$ solution with previously reported catalysts.

Catalysts	**T (K)**	***n*(H_2+N_2)/ *n*($N_2H_4BH_3$)**	**TOF (h^{-1})**	**NaOH (M)**	**Ref**
$Ni_{0.9}Pt_{0.1}$-MoO_x/NH_2-N-rGO	323	6	4412	1.5	S4
$Ni_{0.9}Pt_{0.1}$-CeO_x/MIL-101	323	6	2951.1	1.0	S5
Ni@Ir/OMS-2	323	6	2590	5.0	S6
$Rh_{0.5}$-$(MoO_x)_{0.5}$	323	6	2000	2.0	S7
$Ni_{0.9}Pt_{0.1}$/MIL-101	323	6	1515	0.5	S8
$Ni_{0.75}Ir_{0.25}$/$La_2O_2CO_3$	323	6	1250	1.2	S9
$Rh_{0.8}Ni_{0.2}$/MIL-101	323	6	1200	0.5	S10
Ni-MoO_x/BN	323	6	600	1.0	S11
Ni-Cr/CTO-NF	**323**	**6**	**555**	**3**	**This work**
$Ni_{0.6}Pd_{0.4}$-MoO_x	323	6	405	2.0	S12
$Ni_{0.5}Fe_{0.5}$-CeO_x/MIL-101	343	6	351.3	3.6	S13
$Ni_{0.9}Pt_{0.1}$-CeO_2	323	5.74	234	0.5	S14
$Cu_{0.6}Ni_{0.4}Mo$	323	6	108	2.0	S15
Rh_4Ni_1 NPs	323	5.8	90.0	--	S16
$Ni_{0.36}Fe_{0.24}Pd_{0.4}$/MIL-101	323	6	60	2.0	S17
$Ni_{0.89}Pt_{0.11}$ NPs	323	5.79	18.0	--	S18

References

S1 Z. J. Zhang, Y. Q. Wang, X. S. Chen, and Z. H. Lu, Facile synthesis of NiPt-CeO_2 nanocomposite as an efficient catalyst for hydrogen generation from hydrazine borane. *J. Power Sources,* 2015, **291**, 14–19.

S2 Q. L. Yao, Z. H. Lu, R. Zhang, S. L. Zhang, X. S. Chen, and H. L. Jiang, A noble-metal-free nanocatalyst for highly efficient and complete hydrogen evolution from $N_2H_4BH_3$. *J. Mater. Chem. A,* 2018, **6**, 4386–4393.

S3 W. Wang, X. L. Hong, Q. L. Yao, and Z. H. Lu, Bimetallic Ni-Pt nanoparticles immobilized on mesoporous N-doped carbon as a highly efficient catalyst for complete hydrogen evolution from hydrazine borane. *J. Mater. Chem. A,* 2020, **8**, 13694.

S4 X. Kang, J.X. Yao, Y. X. Duan, Z. Y. Chen, J. M. Yan, and Q. Jiang, Supported ultrafine NiPt-MoO_x nanocomposites as highly efficient catalysts for complete dehydrogenation of hydrazine borane. *J. Mater. Chem. A,* 2021, **9**, 26704–26708.

S5 Y. X. Bai, Y. B. Liu, H. N. Shang, S. J. Li, and J. S. Liang, MIL-101 supported CeO_x-modified NiPt nanoparticles as a highly efficient catalyst toward complete dehydrogenation of hydrazine borane. *New J. Chem.,* 2022, **46**, 13971–13980.

S6 M. Yurderi, T. Top, A. Bulut, G. S. Kanberoglu, M. Kaya, and M. Zahmakiran, Complete dehydrogenation of hydrazine borane on manganese oxide nanorod-supported Ni@Ir core-shell nanoparticles. *Inorg. Chem.,* 2020, **59**, 9728–9738.

S7 Q. L. Yao, M. He, X.L. Hong, X. Y. Chen, F. Guo, and Z. H. Lu, Hydrogen production via selective dehydrogenation of hydrazine borane and hydrous hydrazine over MoO_x-promoted Rh catalyst. *Int. J. Hydrogen. Energy*, 2019, **44**, 28430–28440.

S8 Z. J. Zhang, S. L. Zhang, Q. L. Yao, X. S. Chen, and Z. H. Lu, Controlled synthesis of MOF-encapsulated NiPt nanoparticles toward efficient and complete hydrogen evolution from hydrazine borane and hydrazine. *Inorg. Chem.,* 2017, **56**, 11938–11945.

S9 X. L. Hong, Q. L. Yao, M. L. Huang, H. X. Du, and Z. H. Lu, Bimetallic NiIr nanoparticles supported on lanthanum oxy-carbonate as highly efficient catalysts

for hydrogen evolution from hydrazine borane and hydrazine. *Inorg. Chem. Front.,* 2019, **6**, 2271–2278.

S10 Z. J. Zhang, S. L. Zhang, Q. L. Yao, F. Guo, M. H. Zhu, and Z. H. Lu, Metal–organic framework immobilized RhNi alloy nanoparticles for complete H_2 evolution from hydrazine borane and hydrous hydrazine. *Inorg. Chem. Front.*, 2018, **5**, 370–377.

S11 S. J. Li, X. Kang, B. R. Wulan, X. L. Qu, K. Zheng, X. D. Han, and J. M. Yan, Noble-metal-free Ni-MoO_x nanoparticles supported on BN as a highly efficient catalyst toward complete decomposition of hydrazine borane. *Small Methods,* 2018, **2**, 1800250.

S12 Q. L. Yao, K. K. Yang, W. D. Nie, Y. X. Li, and Z. H. Lu, Highly efficient hydrogen generation from hydrazine borane via a MoO_x-promoted NiPd nanocatalyst. *Renew. Energy,* 2020, **147**, 2024–2031.

S13 S. J. Li, H. L. Wang, B. R. Wulan, X. B. Zhang, J. M. Yan, and Q. Jiang, Complete dehydrogenation of $N_2H_4BH_3$ over noble-metal-free $Ni_{0.5}Fe_{0.5}$-CeO_x/MIL-101 with high activity and 100% H_2 selectivity. *Adv. Energy Mater.*, 2018, **8**, 1800625.

S14 Z. J. Zhang, Y. Q. Wang, X. S. Chen, and Z. H. Lu, Facile synthesis of NiPt–CeO_2 nanocomposite as an efficient catalyst for hydrogen generation from hydrazine borane. *J. Power. Sources,* 2015, **291**, 14–19.

S15 Q. L. Yao, Z. H. Lu, R. Zhang, S. L. Zhang, X. S. Chen, and H. L. Jiang, A noble-metal-free nanocatalyst for highly efficient and complete hydrogen evolution from $N_2H_4BH_3$. *J. Mater. Chem. A*, 2018, **6**, 4386–4393.

S16 D. C. Zhong, K. Aranishi, A. K. Singh, U. B. Demirci, and Q. Xu, The synergistic effect of Rh–Ni catalysts on the highly-efficient dehydrogenation of aqueous hydrazine borane for chemical hydrogen storage. *Chem. Commun.,* 2012, **48**, 11945–11947.

S17 K. Yang, K. K. Yang, S. L. Zhang, Y. Luo, Q. L. Yao, and Z. H. Lu, Complete dehydrogenation of hydrazine borane and hydrazine catalyzed by MIL-101 supported NiFePd nanoparticles. *J. Alloy Compd.,* 2018, **732**, 363–371.

S18 J. L. Hannauer, O. Akdim, U. B. Demirci, C. Geantet, J. M. Herrmann, P. Miele,

and Q. Xu, High-extent dehydrogenation of hydrazine borane $N_2H_4BH_3$ by hydrolysis of BH_3 and decomposition of N_2H_4. *Energy Environ. Sci.,* 2011, **4**, 3355–3358.